Magnetic levitation using high temperature superconducting pancake coils as composite bulk cylinders

2015 Supercond. Sci. Technol. 28 115007

(http://iopscience.iop.org/0953-2048/28/11/115007)

OPEN ACCESS
IOP Publishing
Superconductor Science and Technology
Supercond. Sci. Technol. **28** (2015) 115007 (10pp)
doi:10.1088/0953-2048/28/11/115007

Magnetic levitation using high temperature superconducting pancake coils as composite bulk cylinders

A Patel[1], S C Hopkins[1], A Baskys[1], V Kalitka[2], A Molodyk[2] and B A Glowacki[1,3,4]

[1] Department of Materials Science and Metallurgy, University of Cambridge, 27 Charles Babbage Road, Cambridge, CB3 0FS, UK
[2] ZAO SuperOx, 20-2 Nauchny Proezd, Moscow, Russia
[3] Department of Physics and Energy, University of Limerick, Plassey, Ireland
[4] Institute of Power Engineering, ul. Mory 8, 01-330 Warsaw, Poland

E-mail: ap604@cam.ac.uk

Received 9 June 2015, revised 10 August 2015
Accepted for publication 21 August 2015
Published 25 September 2015

Abstract

Stacks of superconducting tape can be used as composite bulk superconductors for both trapped field magnets and for magnetic levitation. Little previous work has been done on quantifying the levitation force behavior between stacks of tape and permanent magnets. This paper reports the axial levitation force properties of superconducting tape wound into pancake coils to act as a composite bulk cylinder, showing that similar stable forces to those expected from a uniform bulk cylinder are possible. Force creep was also measured and simulated for the system. The geometry tested is a possible candidate for a rotary superconducting bearing. Detailed finite element modeling in COMSOL Multiphysics was also performed including a full critical state model for induced currents, with temperature and field dependent properties and 3D levitation force models. This work represents one of the most complete levitation force modeling frameworks yet reported using the H-formulation and helps explain why the coil-like stacks of tape are able to sustain levitation forces. The flexibility of geometry and consistency of superconducting properties offered by stacks of tapes, make them attractive for superconducting levitation applications.

Keywords: magnetic levitation, HTS tape, magnetic bearing, stack of tapes, composite bulk superconductor

(Some figures may appear in colour only in the online journal)

1. Introduction

Stacks of high temperature superconducting (HTS) tapes have proven potential to act as composite superconducting bulks, for either trapped field magnets or as passive components of a magnetic levitation system. Experiments on stacks made from standard 12 mm wide commercial tape have shown that high fields can be trapped using both the pulsed field method of magnetization [1], and field cooling [2], with work also done on stacking annuli made from larger width tape to form a uniform field persistent magnet, magnetized using field cooling [3, 4].

Superconducting levitation offers stable contactless bearings, enabling very low loss and resistance to sudden failure compared to active magnetic bearings [5]. It is standard to use HTS (RE)$Ba_2Cu_3O_{7-d}$, ((RE)BCO) bulk superconductors, where 'RE' stands for rare earth, for magnetic levitation, but stacks or blocks made from HTS tape have previously been investigated in the context of maglev applications showing that stable levitation of RE permanent magnets (PMs) is possible [6, 7]. There are still many possible configurations involving different geometries and stacking patterns that have yet to be investigated quantitatively for magnetic levitation using stacks of tape. Investigation of levitation performance below 77 K and using the latest commercially available tape has also yet to be reported. Recent production of solder coated tape by SuperOx has allowed for the creation of soldered self-supporting slabs with high geometric tolerance, and previous work by the current authors has shown these soldered stacks are well suited to acting as trapped field magnets [8, 9]. The two main advantages of using stacks of commercial HTS tape for superconducting levitation instead of conventional (RE)BCO bulks are (i) predictability and uniformity of the superconducting properties and (ii) flexibility of geometry. The first advantage has already been exploited in the context of trapped field magnets but the second has not been exploited much. The work reported in this paper uses stacks of tape in a completely different geometry to that of slabs and blocks considered previously. By coiling the tape a cylindrical geometry can be created, suited to cylindrical type superconducting bearings. Cylindrical bearings have previously been used for large scale flywheel energy storage systems such as the one produced by ATZ GmbH [10]. The superconducting stator part is made of many tessellated (RE)BCO bulk pieces to form an approximate cylinder. The rotor is made of a stack of rare-earth PMs giving a final axial levitation force density of 13 N cm^{-2} which is around the maximum that can practically be achieved in such cylindrical superconducting bearings using rare-earth PMs. The geometry of the system presented here is similar to the ATZ bearing because it is targeted at superconducting bearings for applications such as flywheel energy storage and turbo-machinery. The other, planar geometry for superconducting bearings, used in applications like the Boeing flywheel energy storage system [11], involves tessellating hexagonal (RE)BCO bulks to form a planar disk-shaped superconducting stator. The present authors are also working on applying stacks of tape to form planar slabs suitable for this type of bearing geometry, to be reported in future publications.

2. Experimental levitation force measurements

2.1. Superconducting tape specifications and coil geometry

In order to create a cylindrical type levitation force system, 12 mm wide superconducting tape produced by SuperOx [12] was wound into three single pancake coils and the coils stacked on top of each other to form the cylinder shown in figure 1. The two ends of the individual winding are not electrically joined to anything, so the tape is unable to carry any net transport current, so the pancake coils are not acting as current carrying solenoid coils. The coils were wound onto a tufnol former as shown in figure 2. Two Nd-Fe-B PMs

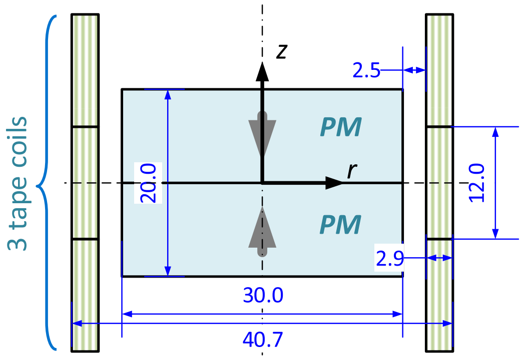

Figure 1. Schematic showing the experimental geometry with a pair of permanent magnets coaxially aligned inside three tape coils (wound around the z-axis) in the field cooling position.

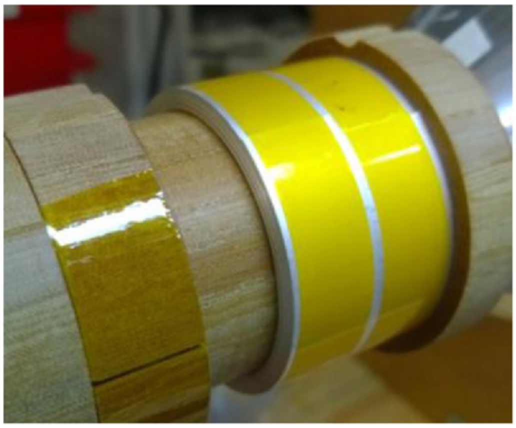

Figure 2. Former with two of the three tape coils already wound.

30 mm in diameter were stacked together and coaxially aligned with the tape coils, as shown in figure 1, by inserting them into a thin-walled stainless steel tube and then forcing them into contact by turning a screw attached to one end of the tube. This typical arrangement produces high magnetic field gradients for the superconductor to maximize stiffness. The centrally aligned position shown in figure 1, was always used for field cooling of the superconducting coils before any movement, and so is associated with the $z = 0$ position in later graphs. Movement only occurred for positive z displacement but force behavior is expected to be the same if moving in negative z due to the symmetry of the coils and PMs in the $z = 0$ plane. The gap between the PMs and coil was 2.5 mm, which is the same as that in the ATZ bearing [10].

The tape used had a nominal minimum I_c rating of 430 A at self-field and 77 K but the average I_c was closer to 500 A. The basic architecture of the tape is similar to that produced by several other manufacturers. The tape is based on a 60 μm thick Hastelloy substrate, with the functional layers deposited by the IBAD-MgO/PLD-GdBCO route. The stabilizer consisted of a 2 μm silver layer, giving a total tape thickness of approximately 65 μm. A total length of 14.1 m of tape was used to create the three pancake coils which each had 39 layers. There was no turn-to-turn insulation or any insulation between the coils. Although this allows transient currents to flow between tape layers, the force measurements were more quasi-static than dynamic and so the effects of these currents is assumed to be negligible for the results reported. The critical state model, reported in section 3.3, predicted the maximum depth over which currents would be induced to be 2.9 mm for a uniform superconducting cylinder at 77.4 K. The thickness of the coil was chosen to be approximately the same, however is it only a first approximation and should not be considered as experimentally optimum given important differences between the tape coils and a uniform, axially symmetric superconducting cylinder (see section 3.5).

The levitation force system was built around an Oxford Instruments Variox cryostat with indirect cooling of the coil samples via helium gas between a cold head and the samples. Full details of the levitation force system can be found elsewhere [13].

2.2. Three layer 'coil' force hysteresis

After cooling of the tape coils to the desired operating temperature in the position shown in figure 1, the PM stack was displaced upward by 40 mm (extraction) and then back down 40 mm (insertion) to the starting position, moving at speeds upto 1 mm s^{-1}, pausing every 0.2 mm for load cell measurement. This resulted in the hysteresis curves shown in figure 3 for the three temperatures tested. It is clear that the temperature has a strong influence on the hysteresis, as expected, with the lowest temperatures exhibiting the smallest hysteresis due to high J_c. Conversely 77.4 K shows highly irreversible behavior, suggesting large-scale penetration of the flux originating from the PM inside the tape coil. Most of the features of the lower temperature curves are very similar to those measured for a PM stack inside a uniform MgB_2 bulk cylinder [14], which is a good system to compare to due to the uniform properties of MgB_2 bulks. The study in [14] measured peak forces of between 150 and 400 N depending on the number of PMs used, at approximately 20 K for an MgB_2 cylinder of 25 mm internal diameter. The peak force measured for the tape coils in the present study was 317 N at 20 K, which proves that comparable axial forces can be sustained by the new system compared to bulk systems. The peak force is very close to the theoretical maximum of 327 N predicted by the perfectly trapped flux (PTF) model which considers infinite J_c. In this respect, the system has very high performance but its stiffness is expected to be lower than the PTF model as the force gradient is clearly lower for the initial displacement. For a bearing application, stability is required which corresponds to a negative gradient on the hysteresis curve. This means that the present system would be operated at 5 mm displacement, for example, if supporting a static axial load such as a flywheel. This gives enough margin for stability if displaced further. Force behavior for displacements greater than, say, 10 mm for this system are not of much practical significance. A full comparison of the results to what is expected from modeling is given in section 3.

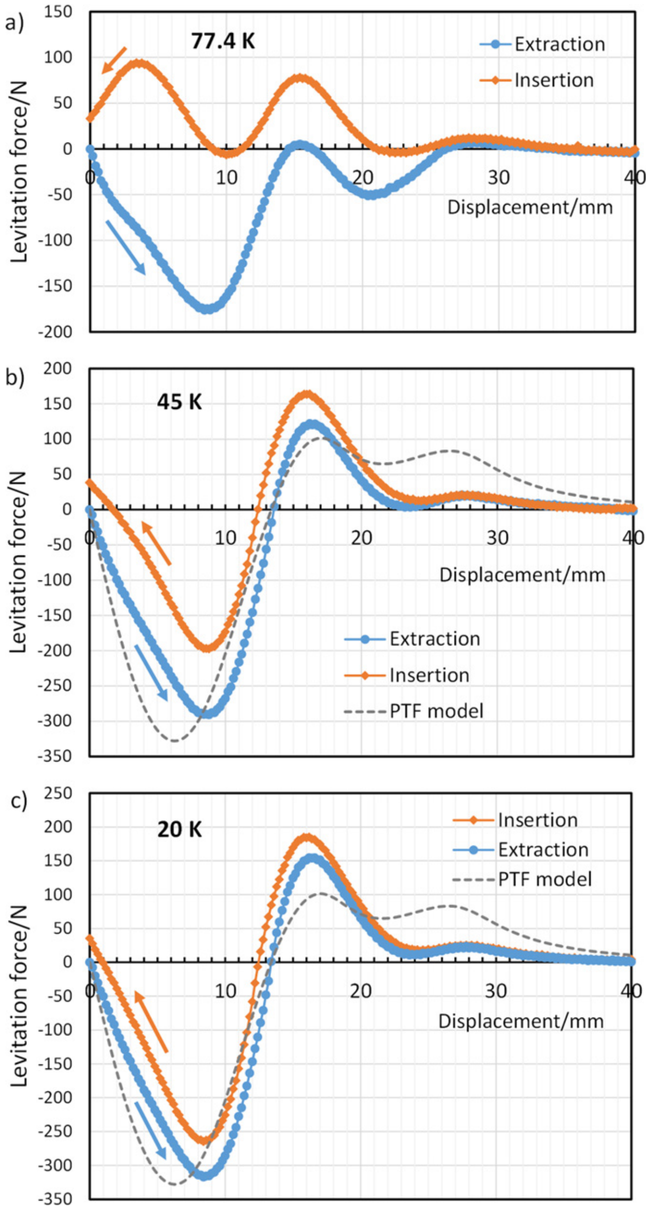

Figure 3. Experimental hysteresis levitation force curves following field cooling at various temperatures. Dotted line for PTF simulation assumes infinite J_c. Arrows represent movement direction.

2.3. Force creep

Force creep, $F(t)$, was measured by displacing the PM stack from the field cooling position by 5 mm, and then recording the change in force with the displacement fixed at 5 mm. This is slightly different to a gap decay measurement for a levitation system, where the load or force is kept constant and the change in the displacement (gap) measured. Whilst the latter is perhaps more directly relevant for a bearing, it was not possible to measure in our system and force decay is still an important indicator of the order of magnitude decay rates for the gap. Because the origin of force creep is flux creep, we expect the force creep to follow the same logarithmic decay observed for flux creep in coils and magnetized bulks. This

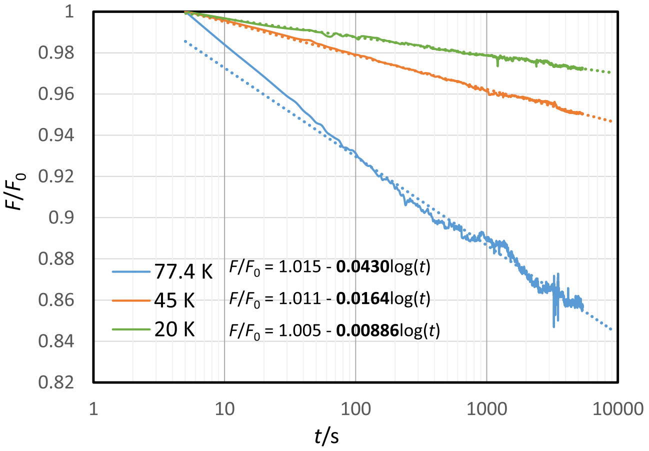

Figure 4. Force creep observed at 5 mm displacement of PMs. F_0 is the force measured 5 s after reaching 5 mm. Creep rates estimated with logarithmic fits (dotted lines).

takes the form:

$$\frac{F(t)}{F_0} = 1 - a \log\left(\frac{t}{t_0}\right) = 1 + a \log t_0 - a \log t, \quad (1)$$

where F_0 is the initial force at time t_0, and a, which is defined as the creep rate, gives the fractional decay in force per time decade expressed by equation (1). The force decay was measured at the same three temperatures used for the previous hysteresis measurements, with force measured every 5 s starting 5 s after reaching a 5 mm displacement. The full experimental results are shown in figure 4, with all temperatures fitting the expected logarithmic decay quite well. This behavior agrees with previous literature on logarithmic force relaxation measured for superconducting bulks [15, 16]. The 77.4 K curve appears slightly non-logarithmic for the first two minutes and later on suffers from noise and drift. The drift is believed to be due to temperature fluctuations as the J_c is sensitive to fluctuations at high temperatures. It is clear that there is an large difference in the fitted creep rate for the highest and lowest temperatures, approximately a factor of 5. Whilst the creep rate was 4.3% per time decade for 77.4 K, it was only 0.89% for 20 K. Given the logarithmic nature of the decay and the very low creep rates for 45 K and lower, the measured force decay behavior is not a concern for the majority of applications. It may also be less of an issue than expected for applications such as flywheels where the levitating body is not rigidly constrained, because creep rates are believed to be significantly lower for bodies which are allowed free oscillations [17].

3. Modeling of superconducting levitation force

Two different FEM techniques were used to simulate and understand the levitation force experiments. The PTF model as described in [18, 19] estimates levitation forces involving superconducting domains by perfectly preserving the magnetic flux density inside the domain when there is movement. This is physically equivalent to an infinite J_c and therefore induced surface currents. It was achieved here by preserving the magnetic vector potential in the superconducting domain as in [20, 21] and is a simple and fast computation tool using a time independent solver. Due to the limited fields produced by rare earth PMs, it is often a good approximation, but breaks down if the J_c is not high enough.

The critical state model [22], on the other hand, simulates real induced currents within the superconducting domain and so is a more accurate tool and is necessary to determine current flow paths, however computation times are considerably longer than the PTF model and numerical instability is a frequent problem.

3.1. Modeling parameters for the critical state model

The H-formulation for magnetic fields was used in COMSOL Multiphysics 5.0. The framework used an *E–J* power law to simulate the critical state, where E_ϕ and J_ϕ are the azimuthal electric field and current density respectively.

$$E_\phi = E_0\left(\frac{J_\phi}{J_c(B, T)}\right)^n. \quad (2)$$

The Kim model [23] with temperature dependent parameters was used to describe the dependence of the critical current density (equivalent to the engineering critical current density J_e for the experiment) on field:

$$J_c(B, T) = J_e = \frac{I_{c0} L_0(T)}{wd\left[1 + B/B_0(T)\right]}. \quad (3)$$

A full description of the parameters used is given in table 1. The motivation behind equation (3) is to use a simple mathematical framework that can easily fit typical measured J_e values for commercial superconducting tape over 10–77 K and fields of 0–4 T, as these are the ranges of interest for superconducting bearings. The temperature dependent lift factor is defined below, where SF is the self field, and I_c refers to tape critical current.

$$L_0(T) = \frac{I_c(T, B = 0)}{I_c(77.4K, SF)}. \quad (4)$$

Lift factors generally describe the I_c of commercial HTS tape at different temperatures and/or applied fields compared to the I_c at 77.4 K and in self-field which is considered the standard performance parameter. In this case, the field dependence is described by the Kim model in equation (3) so the lift factor used describes the effect of temperature on I_c only at zero-field rather than self-field, even though this condition is impossible in conventional critical current measurements. Zero field J_c has to be defined in modeling and is related to the I_c values for which the fitting curves for $I_c(B)$ data, intercept the I_c axis. Therefore, equation (4) gives an L_0 slightly greater than 1 for 77.4 K. Both the L_0 factor and the B_0 Kim law parameter, were fitted to data for typical SuperOx tape at different temperatures (available at [24]) and then approximated with a linear temperature dependence given in

Table 1. Descriptions and values of parameters used in modeling.

Parameter	Description	Value
E_0	Electric field constant in equation (2)	1×10^{-4} V m^{-1}
$I_{c0} = I_c$(77 K, SF)	Tape critical current at 77.4 K and self-field	500 A
$L_0(T)$	Lift factor for tape I_c defined by equation (4)	$-0.135T + 11.725$
w	Tape width	12 mm
d	Tape thickness	65 μm
$B_0(T)$	Flux density constant in equation (3)	$-0.0103T + 0.9888$
n	n-value in equation (2)	9 during 'movement', $n(B,T)$ during force creep
n_0	n-value constant in equation (5)	30
T_{0n}	Temperature constant in equation (5)	77.4 K
B_{0n}	Flux density constant in equation (5)	0.75 T
T	Temperature for superconducting domain	20, 45 or 77.4 K
v	Speed of PM movement in model and experiment	1 mm s^{-1}

table 1 to give $B_0(T)$ and $L_0(T)$. The Kim model used data for which applied field is always perpendicular to the tape surface, hence $J_c(\theta)$ anisotropy is ignored in our model. These linear dependencies actually fit the data quite well whilst keeping the dependence as simple as possible. It should be noted that the empirically reliable linear approximation made for $L_0(T)$ is different from the typical zero-field temperature dependence of J_c used more in the context of bulk superconductors as described in [25]. The n-value was constant during the 'movement' part of the modeling, but had a field and temperature dependence given below for the flux creep part of the models during which there is no domain movement.

$$n(B, T) = \frac{n_0}{1 + B/B_{0n}}\left(\frac{T_{0n}}{T}\right). \tag{5}$$

A constant and low $n = 9$ value, as used in [26], was reliable for the movement part (as justified in section 3.3) but not for flux creep, which is very sensitive to the n-value used. Therefore a full temperature and field dependence was used, fitting data such as [27] for high temperatures. Full lower temperature data is lacking in literature so the fit is very approximate for lower temperatures.

The movement of the PMs was implemented by modeling the PMs as a thin layer of current density on the circumferential surface based on the theoretical equivalence of remanent magnetization and surface current density for a PM: $J_s = B_{rem}/\mu_0$ (A m^{-1}). The thin layer currents approximating the ideal surface current density J_s, were then moved along the z direction by defining them with a time and space dependent current density $J(z,r) = J_0(vt,r)$ (A m^{-2}), where v is the speed at which the domain moves and was 1 mm s^{-1} for both experiment and model. The H-formulation in COMSOL does not allow true surface currents to be modeled, nor does it seem possible to move actual domain boundaries, so the method used was the only one feasible and reliable enough, provided a thin enough current layer was used for $J(z,r)$. Lastly, it is worth mentioning that a first approximation of J_c anisotropy was tried to see if this affected the levitation force. A modified Kim law using parallel and perpendicular B components as in [28] was tried, but showed no difference in the force values (less than 1%), so J_c anisotropy was ignored for all subsequent modeling.

3.2. PTF model results

The 2D axially symmetric PTF model was applied to the same geometry as the experimental system shown in figure 1, resulting in the force–displacement curves shown in figures 3(b) and (c). Because the model is equivalent to having infinite J_c, there is no hysteresis in the curves. There is clear correlation between the shape of this curve for an ideal superconducting cylinder and the real experiment. As in the case for previous experiments with bulk superconducting cylinders [20], the PTF model curve approximately gives the maximum stiffness for initial displacement and also the maximum force. This applies to figures 3(b) and (c) where the initial stiffness and largest force magnitude is never higher than that predicted by the PTF model. The critical state model results presented in the next section turned out to be very close in shape and magnitude to the PTF model results, which validates the reliability of the PTF modeling.

3.3. Critical state for uniform superconducting cylinder

A superconducting cylinder was modeled in a 2D axisymmetric geometry with the same overall dimensions as the three tape coils shown in figure 1 combined, and with a constant n value of 9. This is a good first approximation which shows the magnitude and depth over which currents should be induced at different temperatures when moving the PM stack. Figure 5 shows the circulating current density induced in the cross-section of the cylinder wall for the three different temperatures modeled for a displacement of 5 mm. Three different current regions with alternating sign are induced which is related to the existence of 3 effective field poles of the PM stack. When you stack two PMs together with their poles opposing, as in figure 1, you expel flux radially outward from the region joining the two PMs together (see [19] for illustrations of field lines). As this expelled flux is axially symmetric, it can be considered as a single pole. Only two current regions (opposite in sign) would be created

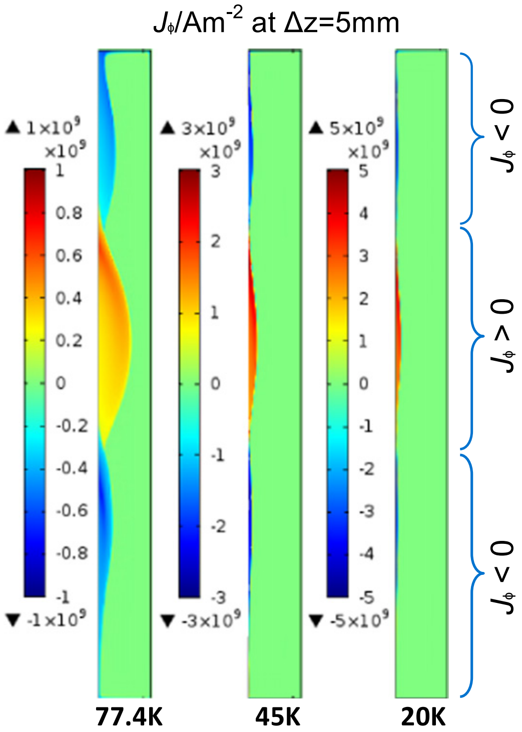

Figure 5. Current densities induced inside the wall of a uniform superconducting cylinder shown on rectangular green cross-sections for different temperatures. The critical state model gives regions of oppositely flowing current density which slightly overlap but are mostly separated along the cylinder length.

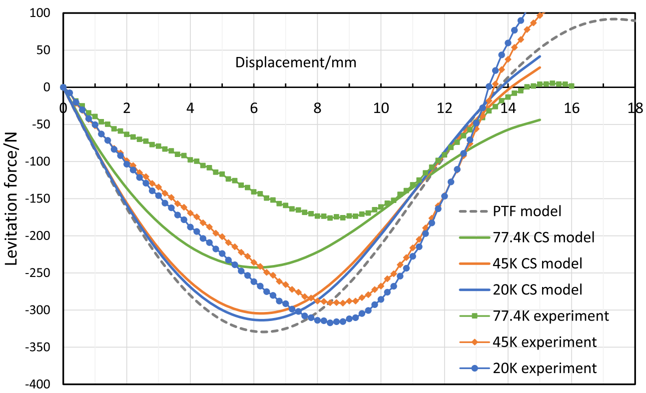

Figure 6. Summary of PTF model, critical state (CS) model and experimental levitation force curves. The CS curves considers a single superconducting cylinder of 36 mm in height.

if there was only one PM which has two poles. The higher the temperature, the lower the J_c and so the greater the depth over which current is induced which relates to large hysteresis. The 77.4 K case therefore explains why significant hysteresis can only be seen for force measurements at high temperature. At 45 K and below, it is clear that the high J_c leads to effective shielding, confining the induced current to a thin layer near the inner surface which can be approximated well by the PTF model. This is illustrated in figure 6, which gives a summary of all the modeling and experimental levitation force curves. Focussing on the modeling, it is clear that the critical state curves have a similar shape as the PTF model and the 20 and 45 K curves also have very similar magnitude to the PTF curve. However the 77 K curve shows significantly lower forces than the PTF model due to large flux penetration resulting from a low J_c. It is worth noting that the 45 K case was also modeled with the full $n(B,T)$ relation but less than 0.5% difference was found in the force curve compared to $n = 9$ curve, proving the reliability of using only $n = 9$ for movement.

The critical state model is a powerful tool in both exploring temperature dependence of levitation force and understanding what currents are responsible for the forces. However, for the specific case of tape coils, figure 6 shows some significant differences in shape of the force curves compared to the modeling. The force magnitudes are similar and correlated to critical state model curves for different temperatures, but the peak in the force occurs for larger displacements giving a lower force gradient for the initial displacement. Also, the difference in modeling and experimental force magnitudes is largest for 77 K, at which the tape properties are supposedly best known. Given the relatively complex geometry of the real tape coils/spirals compared to a uniform cylinder, it is encouraging that there is some real correlation between the modeled and experiment, however the results suggest there are still some differences which can be slightly reduced further by considering splitting the cylinder into three domains and applying current constraints as in section 3.6.

Section 3.5 aims at answering the first and most basic question of how a superconducting domain without directly circulating current paths can sustain large levitation forces. It is worth firstly considering whether the different regions of azimuthally flowing current I_ϕ, cancel out if averaged over the cross-sectional area, as a preliminary to looking at cases where current flow is restricted. This is best quantified by considering the net current for a whole cross-section, divided by the sum of the current magnitudes, which gives the following equation for current mismatch.

$$\frac{\sum I_\phi}{\sum |I_\phi|} = \frac{\iint J_\phi(r, z)\mathrm{d}s}{\iint |J_\phi(r, z)|\mathrm{d}s}. \tag{6}$$

Applying this equation to the critical state model results for the single cylinder (such as those for 5 mm displacement in figure 5) allows the current flow mismatch to be plotted against displacement, as in figure 7. This summary shows that for displacements less than 10 mm, the mismatch is only a few per cent for all temperatures. Although there must be an error resulting from finite mesh element size, the results are convincing enough to say that for the displacements of interest, there is small current flow mismatch.

3.4. Force creep in the critical state

Force creep was also simulated using the critical state model for the single cylinder by calculating time-dependent changes in force after reaching a 5 mm displacement. Given the

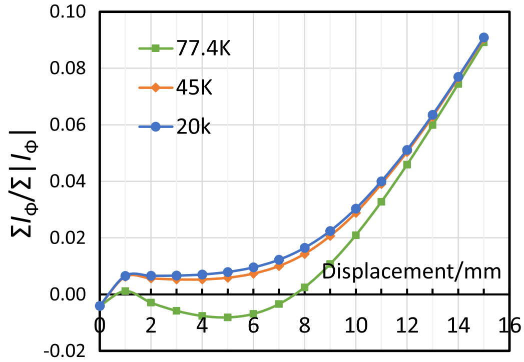

Figure 7. Total current flow mismatch for the cross-section of a single uniform superconducting cylinder.

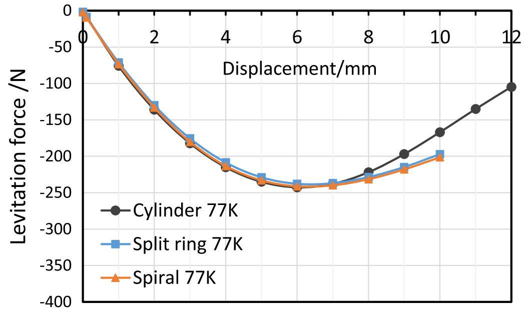

Figure 9. Levitation force for displacement of a PM stack considering the original uniform superconducting cylinder and also a superconducting split ring and spiral with same overall height and inner and outer diameters.

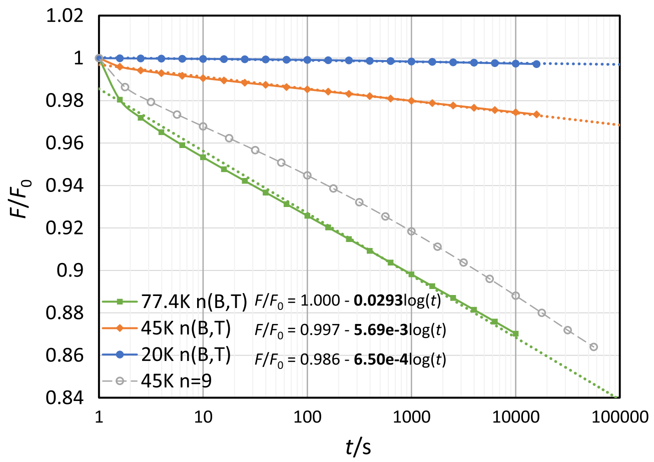

Figure 8. Simulated force creep for the uniform superconducting cylinder after 5 mm displacement of the PMs using estimated $n(B,T)$ relationships. Results for $n = 9$ for 45 K also shown to highlight how large creep is for low n values. Creep rates estimated with logarithmic fits.

sensitivity of force creep to n value, a full $n(B,T)$ relation as described by equation (5) was used, which actually varied between approximately 7 and 50 depending on temperature and local field. The resulting creep behavior is illustrated in figure 8. The creep is logarithmic as expected which matched the type of decay observed experimentally. As for the experimental results in figure 4, there is strong temperature dependence of the creep rate, although all the modeling creep rates are lower than the real ones, significantly so for the lower temperatures. This suggests that the $n(B,T)$ relations are an overestimate for lower temperatures. Given the lack of data for n values, these differences are not too surprising but it would be interesting in future to use accurate n value data for the tape being used which would allow a more direct comparison between the critical state model for levitation, and the experiment. It was interesting to also see what creep rate results from a constant $n = 9$ value which is also shown in figure 8 for 45 K as an example. The rate is much greater than it should be, confirming the need for a temperature dependent n value.

3.5. Critical state for a split ring and superconducting spiral

In order to investigate what happens to current flow for superconducting topologies which do not allow directly circulating current paths, two 3D geometries were modeled with the same overall size as the single uniform cylinder considered previously. A split ring and the simplest possible two-turn spiral were both modeled to determine their force behavior (figure 9) and also current flow paths (figure 10). The force behavior plotted in figure 9 shows that there is very little difference in force up to 7 mm, after which there is some departure compared to the uniform cylinder. These results show that even in theory, geometries such as split rings and spirals do not prevent levitation force and behave very similarly to a complete uniform superconducting domain for displacements up to the largest force. The explanation of these results can be made by considering the current flow mismatch introduced in section 3.3. A very small mismatch should allow the currents flowing in one direction to be diverted into forming the oppositely flowing currents at a boundary, without a difference in the force behavior. In section 3.6 we turn this argument around and impose zero current flow mismatch to 2D axi-symmetric domains and discover that the new solutions for current density do not give largely different forces compared to when there is no constraint, as in all previous models reported in section 3.

Figure 10 displays the geometry and current densities that exist for the split ring and spiral. The 3D models had approximately 0.5 million mesh elements and therefore took over 1 day to solve on a powerful desktop computer. Due to these computational demands, the 2 turn spiral was the most complex geometry that could be practically modeled in this context which represents a coil configuration. Although the real coils have far more turns (39), the two turn model still gives insight into current flow diversion. Figures 10(a) and (b) show the magnitude of the current density flowing next to the geometry surface for a 10 mm displacement (the maximum displacement modeled). Most of the high current density regions are on the inner wall which is not visible in the 3D plots but is clear in (c). Figure 10(c) shows the current flowing through yz plane cross-section. There are clear similarities with the previous uniform cylinder results (like in figure 5) showing that expected current regions have not been

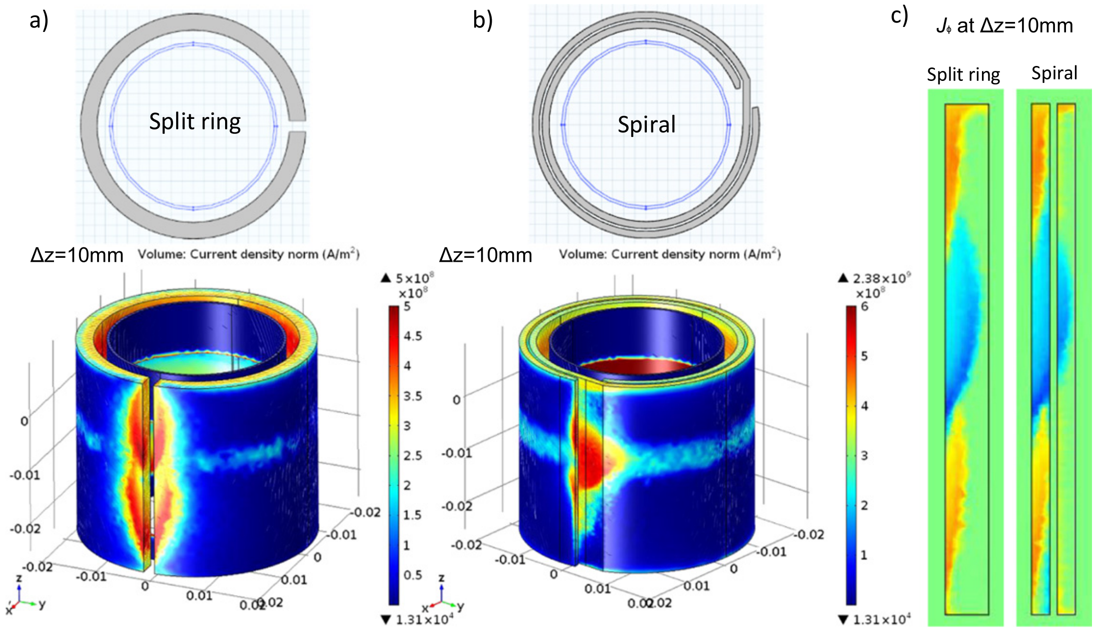

Figure 10. (a) Surface current density for a split ring. (b) Surface current density for a 2 turn spiral. (c) Cross-section through the *yz* plane showing J_ϕ for both cases showing clear similarities. Orange and blue colors represent oppositely flowing currents. Overall split ring and spiral geometry same as previous uniform cylinder.

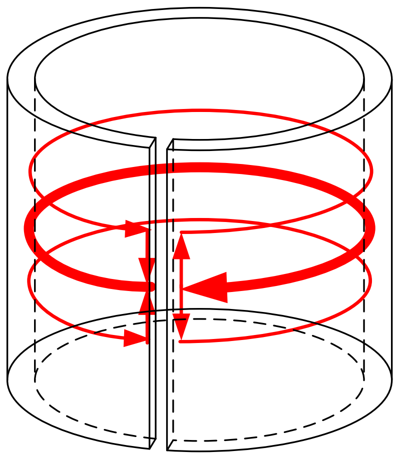

Figure 11. Schematic showing how oppositely induced currents on the inner wall of a superconducting cylinder flow, by being diverted in a perpendicular direction if interrupted by a boundary.

prevented from flowing in either case. The bright areas visible on the outer surface of (a) and (b) therefore correspond to the current diversion regions; the place at which the currents flowing on the inner cylinder wall are being diverted in the *z* direction, spreading out near the interrupting boundaries. For the spiral, this occurs at the layer cross-over as well as at the end of the spiral turns in order to give the distribution shown in figure 10(c), which suggests that such current diversion is occurring in every turn of our real coils. The current diversion for the split ring is more explicitly illustrated in the schematic shown in figure 11.

The 3D results explain why discontinuous superconducting domains do not prevent stable levitation forces, a result evident in most superconducting bearings using segmented (RE)BCO bulks. The results also apply to simple spiral geometries, but are not able to fully explain the difference in levitation force curve seen for the experimental tape coils compared to modeling. The same effects of forced current diversion seen in these 3D models can be approximated by applying current constraints for 2D-axisymmetric models as in the next section

3.6. Critical state for 2D-axisymmetric models with current constraints

Having shown the way in which current is allowed to divert at boundaries for 3D domains, we have demonstrated why split rings and spirals can still sustain levitation forces. Even when there is a strict requirement of no net current flow across the cross-section of a superconducting domain, azimuthally flowing currents can still be set up which are similar to the case of a plain superconducting cylinder. The next step is to try and apply current constraint conditions in 2D-axisymetric models which are simpler to solve, to approximate the behavior of our more complex 3D-geometry. This can be achieved by applying an integral constraint in COMSOL such that the integral of current J_ϕ over the cross-sectional area of a specified domain, is zero at all times. Applying this constraint to the single superconducting cylinder modeled in figure 5 and figure 6 unsurprisingly gives almost no different in the force curve up to 15 mm displacement due to the current flow mismatch already being very small as described in figure 7.

The more relevant and interesting application of current constraints comes when splitting the cylinder into 3 separate cylinders each with the same overall dimensions as the real pancake coils, as this represents our real system more accurately. Without the current constraints, this model would be

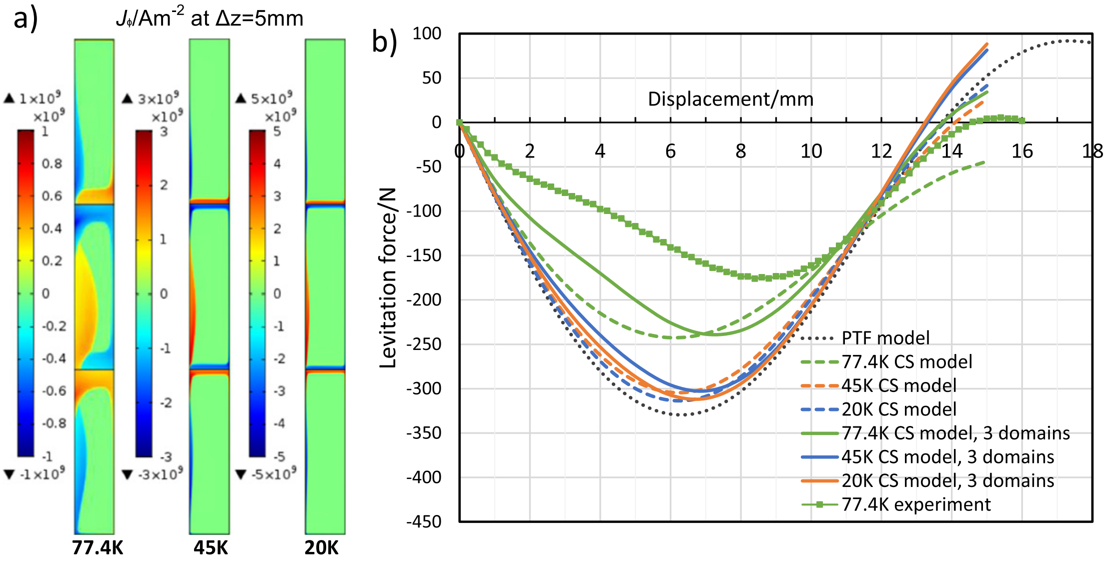

Figure 12. (a) Current densities induced inside a superconducting cylinder split into 3 domains of the same size as each pancake coil, each with a total current constraint. (b) Critical state (CS) force curves for the new segmented current constraint model compared to the previous single cylinder model.

identical to the single cylinder model as the boundaries between the cylinders (for axisymmetric models) have no effect on current flow. Looking at figure 5, it is clear that splitting the cylinder into three will result in domains that have very large current flow mismatch, or indeed current flowing almost only in one direction which we know is not allowed in our coils. The current constraint was therefore applied to each of the three cylinder domains yielding the results shown in figure 12. The induced currents shown in figure 12(a) for 5 mm displacements have similar 3 regions of current seen in figure 5 but now have new regions of current next to the boundaries between coils which are a direct result of current conservation. The effect of these new currents on levitation force can be seen in figure 12(a) compared to the single cylinder critical state model. 45 and 20 K show almost no difference but the 77 K curve is visibly shifted closer to the real experimental curve in figure 6 but a difference still remains. Interestingly this result shows that for our system, having a current constraint alone for the overall superconducting region, has a very small effect on levitation force, but splitting the cylinder into separate cylinders and having a current constraint, can lead to larger changes.

The tape coils are an extreme case of a spiral, where not only does the total current in the spiral cross-section have to be zero (as in figure 12(a)), but the total current in each tape has to be zero. This is effectively imposing an extra constraint similar to stating that the line integral of current density from the top to the bottom of the cylinder, for a given radius, has to be zero. Preliminary results for modeling which splits each of the three cylinders further into thin domains (up to 39 as in our real coils), each with their own current constraint, shows little change in levitation force compared the curves in figure 12(a). This may be due to too coarse a mesh being used for each domain or it may indicate other unknown factors are responsible for the differences between the model and the behavior of the real pancake coils. Three new future experiments using cylindrical geometry may be performed that will help strengthen the reliability of models and increase our understanding of these levitation force systems. A PM stack will be placed inside the following: (1) A plain bulk MgB_2 cylinder similar to that used in [14] which is simplest to model (no current constraints). (2) A single pancake coil using ≈40 mm wide HTS tape. (3) A stack of tape annuli the same as those used in [4] by Hahn *et al* which should give similar results to an MgB_2 bulk cylinder due to lack of current constraints. Although the lack of turn to turn and inter coil insulation are not believed to significantly affect our results due to the quasi-static nature of the measurements, it is worth experimentally check if adding insulation changes the force results.

4. Summary

Stable superconducting levitation is possible between PMs and field cooled coils of commercial superconducting tape which could form the basis of a rotary superconducting bearing. Forces up to 317 N were measured for a stack of three coils with an inner diameter of 35 mm made from 12 mm wide SuperOx tape, which is similar to the maximum force expected for an ideal bulk cylinder. The force creep was investigated at different temperatures and found to be logarithmic with time in all cases. A detailed investigation of levitation force was conducted by extensive FEM modeling in COMSOL. A comparison of the PTF model and critical state models showed when each model is valid, with the critical state model showing explicitly what currents are induced in a superconductor for a levitation force system. After applying the critical state model to the tape coil geometry, the diversion of current at boundaries was demonstrated and used to explain why levitation forces are still established in cases such as the tape coils, where directly circulating current paths are not possible. However, differences between the modeling and experimental curves still exist.

There are numerous winding/stacking arrangements for the tape that have yet to be tried for a cylindrical geometry as well as the first tests on coils for planar geometry bearings. Radial forces may be measured, as well as the creation of cylinders and disks with the tape soldered together. Dynamic force and stiffness behavior will be reported in future publications.

Acknowledgments

The authors would like to acknowledge the financial support of SKF S2M, the magnetic bearing division of SKF, the Isaac Newton Trust, Cambridge and EPSRC.

References

[1] Patel A, Hopkins S C and Glowacki B A 2013 Trapped fields up to 2 T in a 12 mm square stack of commercial superconducting tape using pulsed field magnetization *Supercond. Sci. Technol.* **26** 032001
[2] Patel A, Filar K, Nizhankovskii V I, Hopkins S C and Glowacki B A 2013 Trapped fields greater than 7 T in a 12 mm square stack of commercial high-temperature superconducting tape *Appl. Phys. Lett.* **102** 102601–5
[3] Hahn S, Kim Y, Voccio J P, Song J B, Bascunan J, Tomita M and Iwasa Y 2014 Temporal enhancement of Trapped field in a compact NMR magnet comprising YBCO annuli *IEEE Trans. Appl. Supercond.* **24** 4300805
[4] Hahn S, Kim S B, Ahn M C, Voccio J, Bascunan J and Iwasa Y 2010 Trapped field characteristics of stacked YBCO thin plates for compact NMR magnets: spatial field distribution and temporal stability *IEEE Trans. Appl. Supercond.* **20** 1037–40
[5] Werfel F N, Floegel-Delor U, Rothfeld R, Riedel T, Goebel B, Wippich D and Schirrmeister P 2012 Superconductor bearings, flywheels and transportation *Supercond. Sci. Tech.* **25** 014007
[6] Sass F, Dias D H N, Sotelo G G and de Andrade R 2013 Superconducting levitation using coated conductors *IEEE Trans. Appl. Supercond.* **23** 3600905
[7] Sass F, Dias D H N, Sotelo G G and de Andrade R 2012 Coated conductors for the magnetic bearing application *Phys. Proc.* **36** 1008–13
[8] Baskys A, Patel A, Hopkins S C, Kalitka V, Molodyk A and Glowacki B A 2014 Self-supporting stacks of commercial superconducting tape trapping fields of up to 1.6 T using pulsed field magnetisation *IEEE Trans. Appl. Supercond.* **25** 6600304
[9] Patel A, Baskys A, Hopkins S C, Kalitka V, Molodyk A and Glowacki B A 2015 Pulsed-field magnetization of superconducting tape stacks for motor applications *IEEE Trans. Appl. Supercond.* **25** 5203405
[10] Werfel F N, Floegel-Delor U, Riedel T, Rothfeld R, Wippich D, Goebel B, Reiner G and Wehlau N 2008 250 kW flywheel with HTS magnetic bearing for industrial use *J. Phys.: Conf. Ser.* **97** 012206
[11] Strasik M, Hull J R, Mittleider J A, Gonder J F, Johnson P E, McCrary K E and McIver C R 2010 An overview of Boeing flywheel energy storage systems with high-temperature superconducting bearings *Supercond. Sci. Technol.* **23** 034021
[12] Lee S, Petrykin V, Molodyk A, Samoilenkov S, Kaul A, Vavilov A, Vysotsky V and Fetisov S 2014 Development and production of second generation high T-c superconducting tapes at SuperOx and first tests of model cables *Supercond Sci. Technol.* **27** 044022
[13] Patel A, Giunchi G, Albisetti A F, Shi Y, Hopkins S C, Palka R, Cardwell D A and Glowacki B A 2012 High force magnetic levitation using magnetized superconducting bulks as a field source for bearing applications *Phys. Proc.* **36** 937–42
[14] Perini E and Giunchi G 2009 Field cooling of a MgB_2 cylinder around a permanent magnet stack: prototype for superconductive magnetic bearing *Supercond. Sci. Technol.* **22** 045021
[15] Riise A B, Johansen T H, Bratsberg H and Yang Z J 1992 Logarithmic relaxation in the levitation force in a magnet-high T_c-superconductor system *Appl. Phys. Lett.* **60** 2294–6
[16] Tseng Y S, Chiang C H and Chan W C 2004 Levitation force relaxation in YBCO superconductors *Physica* C **411** 32–4
[17] Smolyak B M and Zakharov M S 2014 On the force relaxation in the magnetic levitation system with a high-T_c superconductor *Supercond. Sci. Technol.* **27** 055018
[18] May H, Palka R, Portabella E and Canders W R 2004 Evaluation of the magnetic field—high temperature superconductor interactions *COMPEL-Int. J. Comput. Math. Electr. Electron. Eng.* **23** 286–304
[19] Patel A, Palka R and Glowacki B A 2011 New fully superconducting bearing concept using the difference in irreversibility field of two superconducting components *Supercond. Sci. Technol.* **24** 015009
[20] Patel A, Pałka R, Glowacki B A, Giunchi G, Figini Albisetti A, Shi Y, Cardwell D A and Hopkins S C 2012 Permanent magnet enhancement of fully superconducting MgB_2-$YBa_2Cu_3O_{7-x}$ bearing *J. Supercond. Nov. Magn.* **26** 923–9
[21] Patel A, Hopkins S C, Giunchi G, Figini Albisetti A, Shi Y, Palka R, Cardwell D and Glowacki B A 2012 The use of an MgB_2 hollow cylinder and pulse magnetized (RE)BCO bulk for magnetic levitation applications *IEEE Trans. Appl. Supercond.* **23** 6800604
[22] Chen D X, Sanchez A, Nogues J and Munoz J S 1990 Bean Kim and exponential critical-state models for high-Tc superconductors *Phys. Rev.* B **41** 9510–2
[23] Kim Y B, Hempstead C F and Strnad A R 1962 Critical persistent currents in hard superconductors *Phys. Rev. Lett.* **9** 306–9
[24] Available: (www.superox.ru)
[25] Ainslie M D and Fujishiro H 2015 Modelling of bulk superconductor magnetization *Supercond. Sci. Technol.* **28** 053002
[26] Patel A and Glowacki B A 2012 Enhanced trapped field achieved in a superconducting bulk using high thermal conductivity structures following simulated pulsed field magnetization *Supercond. Sci. Technol.* **25** 125015
[27] Chudy M, Zhong Z, Eisterer M and Coombs T 2015 n-Values of commercial YBCO tapes before and after irradiation by fast neutrons *Supercond. Sci. Technol.* **28** 035008
[28] Zermeno V M R, Abrahamsen A B, Mijatovic N, Jensen B B and Sørensen M P 2013 Calculation of alternating current losses in stacks and coils made of second generation high temperature superconducting tapes for large scale applications *J. Appl. Phys.* **114** 173901